A Systematic Study of the Influence of Various User Specific and Environmental Factors on Wearable Human Body Capacitance Sensing

Sizhen Bian[1,2](✉) and Paul Lukowicz[1,2]

[1] DFKI, Kaiserslautern, Germany
{Sizhen.Bian,Paul.Lukowicz}@dfki.de
[2] University of Kaiserslautern, Kaiserslautern, Germany

Abstract. Body capacitance change is an interesting signal for a variety of body sensor network applications in activity recognition. Although many promising applications have been published, capacitive on body sensing is much less understood than more dominant wearable sensing modalities such as IMUs and has been primarily studied in individual, constrained applications. This paper aims to go from such individual-specific application to a systemic analysis of how much the body capacitance is influenced by what type of factors and how does it vary from person to person. The idea is to provide a basic form which other researchers can decide if and in what form capacitive sensing is suitable for their specific applications. To this end, we present a design of a low power, small form factor measurement device and use it to measure the capacitance of the human body in various settings relevant for wearable activity recognition. We also demonstrate on simple examples how those measurements can be translated into use cases such as ground type recognition, exact step counting and gait partitioning.

Keywords: Human body capacitance · Electric field sensing · Capacitive sensing · Respiration detection · Gait partitioning · Touch sensing · Ground type recognition · Step counting

1 Introduction

Electric capacitance, defined as the ratio between charge and the resulting electric potential, is a fundamental physical property. For a given object, “self-capacitance” reflects the electric potential with respect to the ground. It depends primarily on the object composition and size but is also significantly influenced by the shape and the spatial relation between the object and ground (Fig. 1). When considering the Human Body Capacitance (HBC), we have a baseline given by the body composition (which is 60% water) and a specific person’s size plus components related to posture, limb motion, the contact surface to the

M. Ur Rehman and A. Zoha (Eds.): BODYNETS 2021, LNICST 420, pp. 247–274, 2022.
https://doi.org/10.1007/978-3-030-95593-9_20

ground and contact with other objects. The latter varying components make *HBC* an interesting modality for on-body sensing as they allow a single quantity to capture complex phenomena ranging from complex postures and motions, through clothing and the composition of the environment (in particular the floor) to physiological parameters such as breathing.

A well-known *HBC* application is the musical instrument Theremin [1,2] where the acoustic volume and pitch are controlled by the distance between limbs and two metal loop antennas. Besides that, *HBC* was finitely explored in specific motion-sensing applications. Arshad et al. designed a floor sensing system to monitor the motion of elderly patients [3] to various gesture monitoring systems. Marco [4] presented a textile neckband for head gesture recognition. Bian [5] showed a capacitive wristband for on-board hand gesture recognition. The background behind is the capacitance between two positions on the skin. The variation of the skin capacitance was used to deduce the neck movement. Cohn [6] took advantage of the *HBC* to detect the arm movement by supplying a conductive ground plane near the wrist.

1.1 Paper Aims

This paper aims to go from individual-specific application to a systemic analysis of how much the body capacitance is influenced by what type of factors and how does it vary from person to person. The idea is to provide a basic form which other researchers can decide if and in what capacitive sensing is suitable for their specific applications. To this end, we have designed and implemented a low-cost, low-power consumption, wearable prototype capable of monitoring the value of the *HBC* when the user is in both static and dynamic (moving, walking) states. We also briefly show in simple illustrative experiments how the property that we investigated can contribute to use cases such as ground type recognition (F-score of 0.63), exact step counting (with 99.4% accuracy, 94.3% with a gyroscope for comparison), gait partitioning (with an accuracy of 95.3% and 93.7% for stance and swing phases, respectively, 93.1% and 90.8% with a gyroscope for comparison).

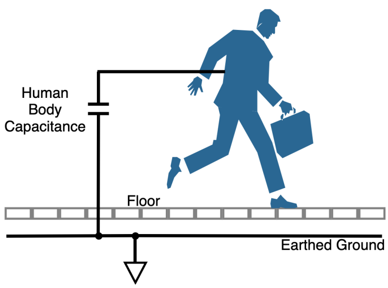

Fig. 1. Human body capacitance: the coupling between body and earthed ground/ surroundings

Table 1. Human body capacitance measurement

Authors/Year	Tool	*HBC* value (pf)	Test condition	Variation source
Bonet et al. [7,8] 2012	Impedance analyzer (10 kHz–1 MHz)	70–110 110–180	Foot on ground Foot 10 cm above ground	Different frequency input of the analyser
Buller et al. [9] 2006	Mathematical model of body-conducive wire mutual capacitance	48.5–48.9	Static standing	Body - wire distance
Forster et al. [10] 1974	Cathode-ray oscilloscope and a shielded resistive probe	100–330	Volunteer lying on medical bed	Laboratory environment
Greason et al. [11] 1995	Mathematical model of ESD and the human body	Qualitative analysis		Grounding, charge sources, etc.
Huang et al. [12] 1997	Capacitive meter	112–113	Sitting on chair	Human body resistance, leakage resistance
Pallas et al. [13] 1991	Oscilloscope and voltage divider probe	120–520	Static standing	Interference from power line
Iceanu et al. [14] 2004	Electrometer (6517A model) and Faraday's cup	160–170 159–165	Static standing Sitting on chair	Different charging voltage from the electrometer
Jonasson et al. [15] 1998	Mathematical model Electrometer (charger sharing method) Conventional AC-bridge (AC-measurement method)	100–300 268 170	Static standing Standing with polymeric soles, linoleum floor Standing with polymeric soles, linoleum floor	Shoes and floor
Fujiwara et al. [16] 2002	Polyhedral model, power charger, analog switch (surface charger method)	120–130	Static standing	Foot-ground distance
Serrano et al. [17] 2003	Physical model, oscilloscope and voltage divider probe	110–3905	Static standing, touching surrounding	Power lines and surroundings
Haberman et al. [18] 2011	Fluke 112 multimeter and customised circuit	110–280	Standing, sitting, touching surrounding	Power lines and surroundings

1.2 Related Work

Research on the measurement of human body capacitance was mainly performed many years ago. Table 1 summarizes the result of such work by different groups. Most of the concluded value matches the definition of the human body capacitance from the Electrostatic Discharge Association (ESDA), in which a value of 100 pF is stated. However, the related explorations are either based on mathematic estimation methods [7,9,15,17], or measured in a laboratory with heavy, expensive instruments, like impedance analyzer, oscilloscope [8,12–14,16]. Besides the theoretical or laboratory methods, all those works focused on the HBC value with a static body state, like sitting, standing, or lying.

To understand how the body capacitance changes in real-time, we developed a wearable, low-cost, low power consumption prototype capable of measuring the value of HBC in real-time (in Sect. 2). We first explored the body capacitance with a static body state, sitting and standing with this prototype. Secondly, we tested the potential influence factors that could change the body capacitance, like the body postures, the wearings like the sole's height, the surroundings like the different indoor spots and ground types (in Sect. 3). Then we observed the body capacitance's real-time change while the tester was in a dynamic state, like walking around a building (in Sect. 4). Finally, we showed several potential applications either quantitively or non-quantitively with our wearable prototype, like exact step counting, gait partitioning, passive touch sensing, respiration monitoring (in Sect. 5).

2 Sensing Approach

Inspired by the Theremin [2], we designed a simple circuit that takes the body as part of it so that the body capacitance could be measured in an straightforward way. Capacitance itself usually is not easy to be measured directly, especially when the sensing unit needs to be portable and battery-powered. Thus, physical variables like the voltage, current, or frequency are adopted as a reflection of the capacitance. Here we put the body into an oscillating circuit, by measuring the frequency of the oscillator, the body capacitance could be deduced. The security is guaranteed when the body is enclosed into the circuit since the current flowing on the skin is in uA level and the voltage in mV level [19].

Figure 2 depicts the timer-based RC oscillator, where the capacitor charges through R1 and R2, discharges through R2. The trigger and threshold terminals are connected so that the oscillator will trigger itself and free run as a multivibrator. The frequency can be calculated by Eq. 1 [20]:

$$f = \frac{1.44}{(R1 + 2 * R2)C} \tag{1}$$

Where C is the capacitance of the parallelly connected $C2$ and $C4$. $C4$ indicates the capacitance of the body. To be noticed, this equation does not account for the propagation delay of the timer as well as the input capacitance of the

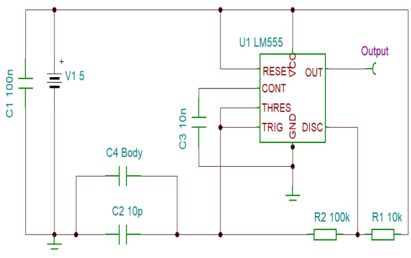

Fig. 2. Human body capacitance sensing front-end

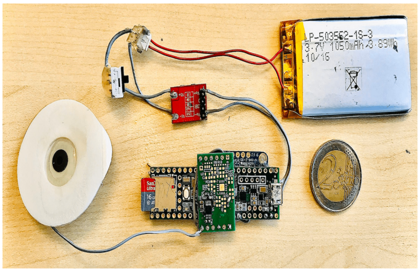

Fig. 3. Hardware prototype

trigger and threshold terminals (around 2 pF each pin). The input capacitance is a particular value, while the propagation delay of the timer will increase with a higher frequency [21]. To address the propagation delay and the pins' input capacitance caused virtual capacitance, we put $C2$ alone in the circuit, and measured an output frequency of 335 kHz, meaning that the virtual capacitance was 10.47 pF. Then we changed $C2$ from 10 pF to 20 pF, got a virtual capacitance of 10.62 pF, which is not too much different from the previous value. Thus in the following experiment, we first read the oscillating frequency, then calculated the body capacitance enclosed into the circuit by subtracting the virtual capacitance of 10.5 pF from the result of Eq. 1.

Figure 3 shows the hardware prototype. The sensing front end is followed by a Teensy 3.6 development board from the market [22], which is capable of counting the frequency up to ten's MHz. The signal data is collected with 10 Hz sample rate and is recorded into an SD card, or transmitted by a low power Bluetooth or a USB cable to the computer. An IMU (BNO055) is also attached to the main board for supplying comparable movement data. The electrode is the universal ECG electrode that can stick on the skin. A 3.7 V lithium battery with 1050 mAh capacity is used to power the hardware after being boosted to 5.0 V. The whole design consumes 85 mA current, where the capacitance measurement part consumes only 2 mA current. The cost for the capacitance measurement part is nothing more than a normal timer as well as a few capacitors and resistors, costing less than one dollar.

A similar front end was used by Tobias [23], where he used a timer-based oscillator for capacitive cm-level proximity sensing. The difference is that the charging and discharging object in the reference was from the environment outside the circuit, namely the capacitance between the electrode and the environment. Another remarkable design was from Cheng's work [24], where the authors used a transistor-based LC oscillator (Colpitts oscillator) for capacitive movement sensing, and focused on the activity recognition. Although an LC-based oscillator enjoys a higher oscillating frequency than RC based timer oscillator, it is less sensitive to the capacitance variation than an RC oscillator, as the frequency of an LC oscillator is inversely proportional to the root of a capacitance.

3 Exploration of HBC in a Static State

We firstly explored the HBC while the body is in a static state: standing and sitting. As Fig. 4 depicts, we had the sensing prototype and a computer for data recording on an office desk, an electrode from the sensing unit was touched by the left hand of the volunteer while the volunteer was sitting on an office chair or standing beside. The prototype was connected to the computer by a USB cable, so they both shared the same ground. The computer was grounded through the power line so that the body was enclosed within the oscillator circuit, as the capacitor $C4$ in Fig. 2 represents. In essence, HBC occurs as a form of an electrostatic field, which is caused by the charge on the body and the charge from the unshielded wiring in the environment. The floor (normally composed of non-conductors like carpet, wood, concrete) itself cannot store charge. When one walks across a floor, the electrostatic charge accumulates on the body. This phenomenon does not implicate the existence of charge stored on the floor. The reason behind locates in the triboelectric effect [25]. That is to say, the dielectrics of the HBC include all the materials between the body and the grounded wires, namely the series of shoes and floor, instead of the shoes alone. This also matches the above mentioned literature [7–18] where all the instruments used to measure the HBC, like the oscilloscope, impedance analyzer, were earthed to the power lines, so as the mathematical or physical models in the literature. The human body model (HBM) in section 3.4.1 of ESD Handbook defined by the ESDA [26] also guarantees the grounded side in a body's physical electric model.

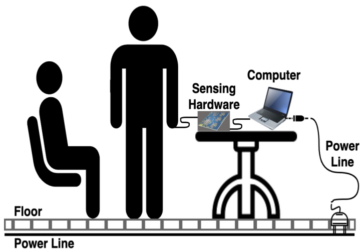

Fig. 4. HBC measurement in static body state

In this experiment, seven participants joined the measurement. Table 2 lists their gender, weight, and height. Table 3 lists the HBC of the volunteers with standing and sitting state. They wore their daily clothes and shoes during this measurement. This measurement was performed in a 4 m × 5 m working office.

Table 2. Volunteers' information

Volunteer	1	2	3	4	5	6	7
Age	31	21	25	25	19	29	28
Gender	Male	Male	Male	Female	Female	Female	Male
Weight (kg)	98	83	71	64	54	58	92
Height (cm)	185	176	168	165	157	161	180

Table 3. *HBC* in standing and sitting

Volunteer	1	2	3	4	5	6	7
Standing frequency (MHz)	0.0580	0.0680	0.0685	0.0680	0.0698	0.0695	0.0655
Standing capacitance (pF)	97.72	80.34	79.60	80.34	77.74	78.16	84.19
Sitting frequency (MHz)	0.0570	0.0664	0.0675	0.0678	0.0672	0.0690	0.0650
Sitting capacitance (pF)	99.80	82.77	81.09	80.64	81.54	78.88	84.99

The measured capacitance from all volunteers shows a value of 77 to 100 pF, which matches the result of previous work, where the HBC was measured by labor used heavy instruments. The capacitance value from all volunteers also shows that the HBC in sitting body state is slightly higher than in the standing state. This is reasonable since the distance from the body to the ground will be shorter by sitting down. The data also shows that volunteers with larger body form (taller and higher weight) have a higher value of HBC, like volunteers one and seven. Volunteers five and six have a smaller body form, and give a smaller standing body capacitance. However, how the body form affects the HBC is not clear at this point, since the body form related cross-objects observation is not acquired with a controlled variable method and also the observation is not common since volunteer two's body form is also big, but he had the same standing body capacitance with volunteer four.

The certain point is that factors like the environment, the wearing, will impact the electrical characteristics of a body. For example, standing against a working grounded refrigerator will form a relatively strong electric field between the body and the appliance. Thus with our simplified HBC meter, we researched the following factors that can affect the HBC by observing the HBC variation within different configurations of a single volunteer.

(A) HBC Influence Factor: Wearing

We firstly focused on the wearing, especially the type and height of sole, which is the main dielectrics that insulate the body from the grounded plane. Four types of soles with two types of material and two sets of height were prepared for the testers. Since it was not easy to find a sole with pure PVC or pure rubber, we took the maximum composition as the sole type. The height of the sole was rounded to the nearest integer number. Table 4 presents the measured HBC with different sole configuration.

Table 4. HBC of different sole height, type with the body standing (unit: pF)

Volunteer	1	2	3	4	5	6	7
bare feet	107.67	91.00	90.10	81.54	88.34	83.39	92.47
2 cm height PVC	95.72	81.54	80.34	79.60	79.46	73.43	89.21
3 cm height PVC	89.21	78.16	78.16	76.08	76.08	69.72	83.39
2 cm height rubber	93.40	77.74	79.60	76.76	78.16	70.32	86.98
3 cm height rubber	90.10	76.76	77.46	76.35	76.08	69.13	85.81

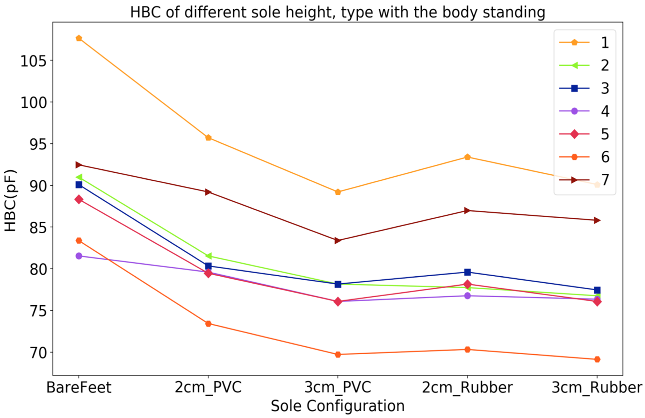

Fig. 5. Seven volunteers' HBC with different sole configuration

Figure 5 depicts a clear HBC variation with different sole configuration for each volunteer. While wearing nothing on the feet, each volunteer gives the highest value of HBC. This value decreases as they wear a thicker sole, which is reasonable since the capacitance value is inversely proportional to the distance between the two corresponding conductive plates. The material types of the sole should also have some influence on the HBC since they have distinct permittivities, but from our data, a clear and uniform difference from the sole material type can not be observed.

(B) HBC Influence Factor: Posture

Besides the wearing, the body postures also play an important role on the HBC, since the postures of the body will change the distance and the overlapping area of the two plates of a capacitor, as Table 3 represents. Besides sitting and standing, we also researched posture variations from the limbs. Table 5 lists the measured capacitance with different postures when the tested volunteer was sitting on the office chair.

The measured capacitance from the seven volunteers locates in the range of 72 pF to 107 pF and shows a uniform variation with the five postures (Fig. 6). Lifting legs will decrease the HBC, the decreased scale can be up to 10 pF, and can be as low as less than 1 pF. It should have something to do with the lifting height that the volunteers performed (unfortunately we didn't instruct the lifting height during the test). Lifting the arm will enlarge the HBC, the reason behind is the enlarged body area relative to the ground. This also explains the result of postures with different distance between the two legs, moving the leg apart will enlarge the HBC.

Table 5. HBC of different postures with the body sitting on the chair (unit: pF)

Volunteer	1	2	3	4	5	6	7
Sitting	99.80	82.77	81.09	80.64	81.54	78.88	84.99
Lift one foot	90.10	78.30	74.08	80.04	76.08	75.00	81.84
Lift two feet	86.64	77.46	73.43	79.17	72.16	73.43	80.79
Lift right arm	104.63	86.81	83.39	81.24	83.39	79.90	90.10
Two legs close to each other	93.78	78.88	74.74	76.08	76.76	77.18	82.15
Two legs apart from each other	106.48	88.34	82.15	81.84	84.19	80.34	89.56

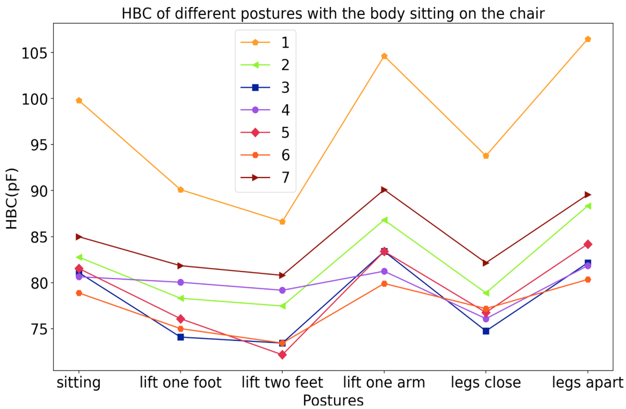

Fig. 6. Seven volunteers' HBC in different body postures

(C) HBC Influence Factor: Environment

Lastly, we tested the influence of the environment, including four ground types. All the objects wore their daily clothes and shoes, stood static in different spots in the office building. Table 6 lists the measured body capacitance value. It is evident that the environment, referring to different spots, different ground types in an office building in this paper, has a significant influence on the HBC while the body is in a static standing state. The largest HBC change was from volunteer one, where around 50 pF was raised while he stood against the wall compared to his standing state in the social hall. The smallest HBC variation was 18.28 pF from volunteer four while she stood against the wall and stood on the wood floor stair.

Table 6. HBC of different environment (unit: pF)

Volunteer	1	2	3	4	5	6	7
Office room	97.72	80.34	79.60	80.34	77.74	78.16	84.19
Against server room door	111.37	103.05	91.91	91.91	83.71	83.08	104.86
Social hall	94.55	77.88	77.74	78.88	77.46	69.72	82.92
Near wall	142.76	113.43	122.35	94.36	95.72	86.64	129.22
Textile floor	99.80	93.03	85.98	77.46	78.88	72.16	95.72
Carpet floor	116.09	102.39	88.34	84.35	84.99	81.84	112.65
Concrete floor	108.88	80.34	81.84	81.84	80.04	78.88	98.13
Wood floor	99.38	74.74	77.46	76.08	74.74	63.12	91.54

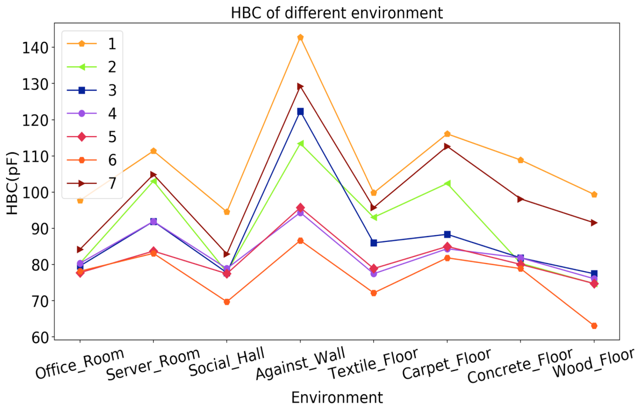

Fig. 7. Seven volunteers' HBC in different environment

Figure 7 depicts the variation of HBC in different environments. The first four spots (office room, near the server room, social hall, and near the wall) had the same textile floor. Each volunteer shows the highest capacitance value while standing against the bearing wall since the solid iron inside the wall is good-coupled with the grounded cables inside the building. The server room is occupied with grounded electric instruments, thus causes a higher HBC while the volunteers stood near the server room's door. At the social hall, all volunteers have the lowest capacitance value compared to the other three spots. The four floor types were chosen since those are pretty common types inside a building.

The textile floor and carpet floor are in the aisle, and the concrete floor locates between the elevator and aisle, the wood floor is the wood stairs between each storey. From the measured capacitance, the body capacitance on the textile floor and concrete floor are different from each other and also do not show a uniform relation among the seven volunteers. The carpet floor gives the highest capacitance value, and the wood floor shows the lowest. However, we can only compare the value measured with the body standing on the carpet and textile floor since they have the same surrounding (wall at both sides), the concrete floor is far from walls, and the wood floor is the stairs. Apparently the body on the carpet floor has higher capacitance than the body on the textile floor, demonstrating that the floor type also affects the HBC.

(D) HBC in static state: briefly summarise

The above-collected data demonstrates that the HBC is not a constant value. The volunteer's wearings, postures, environments are three critical factors that affect the HBC. For example, decreasing the distance between body and ground, enlarging the overlapping area of body and ground, wearing a pair of shoes with a thin sole, standing in an environment where good-grounded metal or wire exists, will enlarge the body's capacitance. This section's study supplied a closer look of the value of HBC in static body state with different wearings, postures, and environment configurations with the low-cost prototype.

4 HBC in Real-Time and Dynamic State

In this section, we recorded the HBC value with a dynamic body state in real-time. Firstly, we cut off the sensing hardware's earthed path so that the volunteers can walk indoors and outdoors without space limitation. Secondly, we stretched the local ground of the sensing unit to the soles with two pieces of wire and conductive tapes (attaching to the underside of the shoe sole). The hardware was worn on the upper back with the sensing electrode attached to the back neck, as Fig. 8 depicts.

4.1 *HBC* While Walking

Since in this wearable way, the prototype only senses the capacitance between body and underside sole, it does not indicate the value of HBC precisely. For verification, we attached the sensing electrode to the floor, and earthed the prototype through the computer, aiming to measure the capacitance between the floor and the earth by averaging the measured one-shot values from over twenty spots of the certain floor type (Fig. 9). Table 7 lists the measured averaged capacitance of different floor types, including the cement brick outside our working building. The value of HBC could be deduced by combining the floor capacitance and the capacitance of the body part measured in the wearable way (when dismissing the tiny step-caused sole-to-ground capacitance).

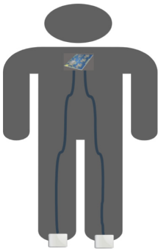

Fig. 8. Body part capacitance measurement in dynamic state

Table 7. Capacitance between floor and earthed ground

Floor type	Textile	Carpet	Concrete (indoors)	Concrete (exit stairway)	Wood	Cement brick (outdoors)
Capacitance (pF)	23.01	30.28	22.36	24.02	24.61	12.54

Fig. 9. Six floor surface types

To address the human body capacitance in a dynamic body state, we worn the prototype and recorded the body part capacitance while the volunteers were walking through the office building. Figure 10 shows five sessions of the recorded capacitance. In the first subplot of Fig. 10, the volunteer started walking on textile (0 s to 9.5 s, 14 s to 19 s, 22.5 s to 24 s) and carpet (9.5 s to 14 s, 19 s to 22.5 s) ground surface, followed by concrete (24 s to 36 s, 48 s to 67.5 s) surface, in between the volunteer went downstairs per wood stairs (36 s to 48 s). Then the volunteer went to the exit stairway and downstairs on the concrete surface (67.5 s to 105 s) for two floors. The outliers in between arose while the volunteer was at the exit stairway's joint spots, near the doors or windows. Finally, the volunteer walked out of the building and wandered around on cement brick ground (105 s to 129 s) for a while.

The body part capacitance of the first volunteer indoors locates in the range of 58 pF to 75 pF. When combined with the floor capacitance listing in Table 7, the HBC will be in the range of 80 pF to 110 pF, which also matches the HBC measured in a static body state. The peak-form signals in Fig. 10 is caused by the swing phase of a gait process, which is like the “lift foot” posture presenting in Table 6, causing around several pico-farads decrease in the body capacitance. Again, each volunteer shows a different value of HBC while the body is in a dynamic state. As explored in the last section, the influence factors could be their body form, postures like step scale, wearing, distance to the wall, etc.

4.2 Classification of Floor Surface Type

As Fig. 10 represents, while walking on different ground surfaces through the office building, the volunteers show regular body capacitance variation. This variation could be used for ground type recognition. We collected 28 sessions of body capacitance variation data from the seven volunteers. Each volunteer walked indoors to outdoors and back with the same path for four times. The interesting point is that the body capacitance variation mode in the exit stairway while walking from indoors to outdoors is significantly distinct with the mode while walking back, as the first two subplots depict (67.5 s to 105 s in the first subplot, vs. 28 s to 65 s in the second subplot). This observation is uniform in all sessions among all volunteers. Thus a potential conclusion can be made that the body capacitance relates not only to where the body is but also to where the body used to be, which will be quantitatively investigated in our future work.

In the HBC based dynamic body state applications, the absolute value of HBC does not matter much. Instead, the variation of the value during different activities is the decisive information. Suppose that the initial body part capacitance (standing on the textile ground surface) were known for each volunteer, so the capacitance value in each session will take the “textile capacitance” as a reference.

We performed the classification without considering the walking direction. In the beginning, we used the sliding window approach to get instances. The size of the window is 1 s, with 0.5 s overlapping. Classical approaches solving the problem of classifying sequences of sensor data involve two steps. Firstly, handcraft the features from the time series data with the sliding windows. Secondly, feed the models with the features and train the models. Different classic machine learning approaches, like k-Nearest Neighbors, Support Vector Machine, Gradient Boosting Machine, were tested, and we chose finally Random Forest model since it provided the best result. All hyper-parameters we used were the default ones by the scikit-learn [27]. We used two procedures to evaluate the classification result.

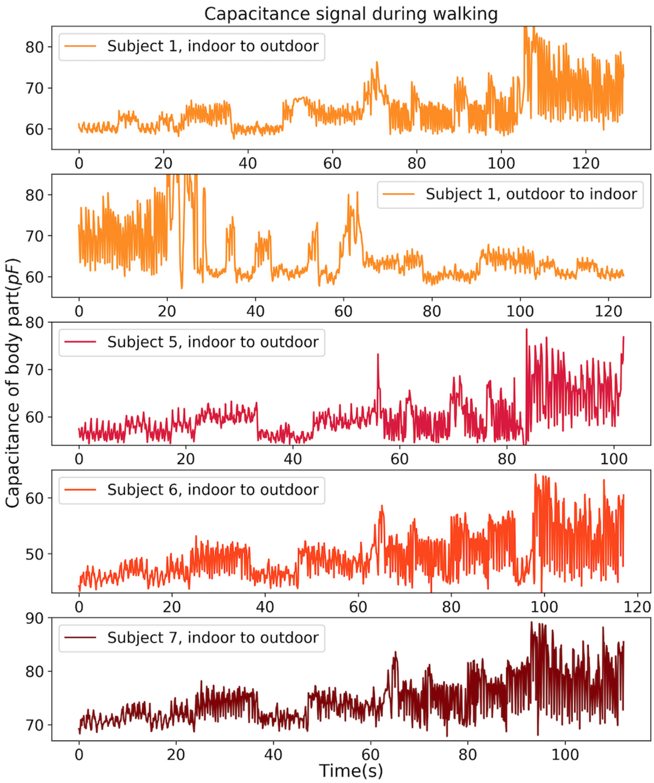

Fig. 10. Body part capacitance while walking around

- Firstly, we evaluated the model by **leaving one session out**, where each of the seven test sessions was selected from the four sessions of each volunteer. The model was then run with four-fold cross-validation.
- Secondly, to test across volunteers classification ability, we employed a **leave one user out** procedure where, for each fold, the test set contains all sessions of one volunteer, while the training set contains all sessions from the remaining volunteers. We run the models with seven-fold cross-validation with one volunteer out.

F-score and accuracy will represent the classification result. At the very beginning of the model procession, we balanced the labels with the method of SMOTE [28] since our data was unbalanced, more instances of the concrete ground type in the exit stairway than instances of the carpet ground type.

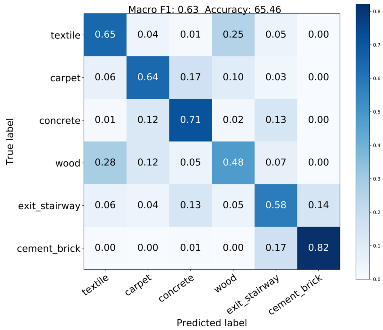

Fig. 11. Leave one session out

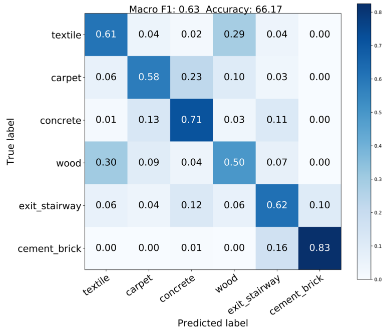

Fig. 12. Leave one user out

The performance of a machine learning model relies on the quality of the feature extraction result [29]. Within each window, we have 10×1 raw data. We summarized the following mathematical features in the time domain: mean, mad, SMA, energy, IQR, entropy, skewness, and kurtosis. We did not consider the spectral domain since all volunteers wandered with a normal walking speed. In total, we utilized eight features, so the input sample was an array of 1×8 per window. The features were then normalized to 0–1.

Figure 11 and Fig. 12 depict the recognition of ground surface types. Overall, by the Random Forest model, a combined F-score of 0.63 is achieved. In both procedures, the outdoor ground type and the indoor concrete ground type have the highest classification rate. The textile surface and wood stairs are the most easily miss-classified types between each other. Considering the HBC influence factors like wearing, body forms, this recognition result is robust and concludes that the HBC signal could be a feasible information source for ground type recognition. Further applications like indoor positioning fusing with other sensing modalities could be explored (when HBC acts as a complementing approach) to reach a higher accuracy, addressing other sensing modalities' drawbacks (like the un-robustness of RF-based approach, drift-accumulation of IMU-based approach).

5 Other Potential Use Cases

Previous sections described how much is the value of HBC in both static and dynamic body states with our sensing unit and demonstrated the prototype's feasibility for HBC monitoring. In this section, we will focus on four potential use cases with this prototype. To be noticed, the following evaluation does not aim to give efficient context recognition based on a large amount of data, but rather at presenting a significant information supplier that can be utilized in future work of human-related interaction and computing.

Fig. 13. Sensing unit on the calf

Since the acquisition of the absolute value of HBC is not necessary in the application field, the contribution will be mainly from how it changes in a dynamic context. Thus we simplified the deployment of our sensing unit to a more portable device. Only one conductive tap was attached to the underside sole, and the hardware was worn on the lower calf instead of the upper back, as Fig. 13 represents.

5.1 Exact Step Counting

Traditional step counting relies on motion sensor [30,31], which is widely used in current wearable devices. However, the accuracy is not guaranteed during the relatively complicated algorithms (removing the noise, abstracting the step information). Our prototype can be an effective approach for exact step counting without any signal noise processing. By wearing the prototype on the lower calf with a local-ground connected conductive tape beneath the sole, the testers walked around the building on the different types of floors. To avoid components damage from accumulated charge while walking, we used an insulated tape to cover the conductive tape. Figure 14 depicts the capacitance measured on the calf and the six axes signals from the IMU. Among the six IMU supplied motion signals, the Z axis from gyroscope supplies the most obvious step information. During each gait procedure (stance phase and swing phase), the prototype sampled an obvious capacitance variation, and this variation information could be used for exact step counting.

As Rhudy et al. [32] summarized in his comprehensive comparison paper, four different step counting techniques were applied to the data from the traditional motion sensing sensor for step counting mostly: peak detection, zero-crossing, autocorrelation method, and fast fourier transform (FFT); and it was determined that using gyroscope measurements allowed for better performance than the typically used accelerometers. Before applying the step counting algorithm, the IMU signals was firstly smoothed by a fourth-order low-pass Butterworth filter with cut-off frequency 4 Hz. Lowpass filters are commonly used in step detection algorithms to reduce undesirable sensor noise [33–35]. In our case, we use the most widely used peak detection method for step counting. Figure 15 shows the detected peaks with the capacitance and gyroscope z-axis data. For the capacitance signal, we detects the peaks simply by checking if the new sampled

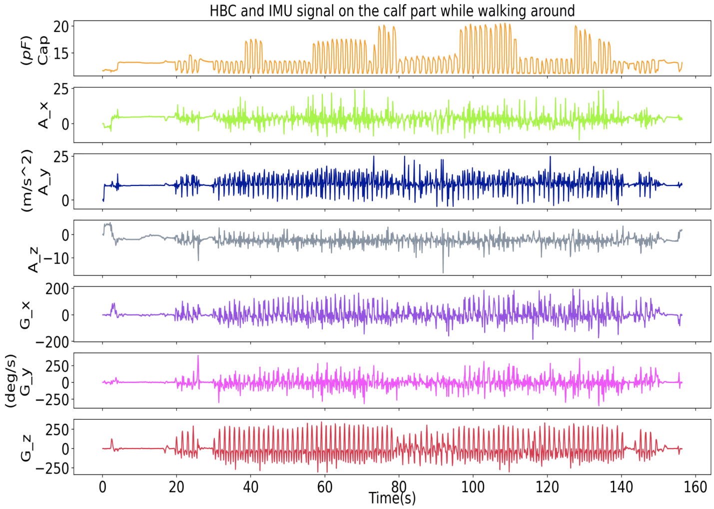

Fig. 14. Capacitance and IMU signal on the calf part while walking around

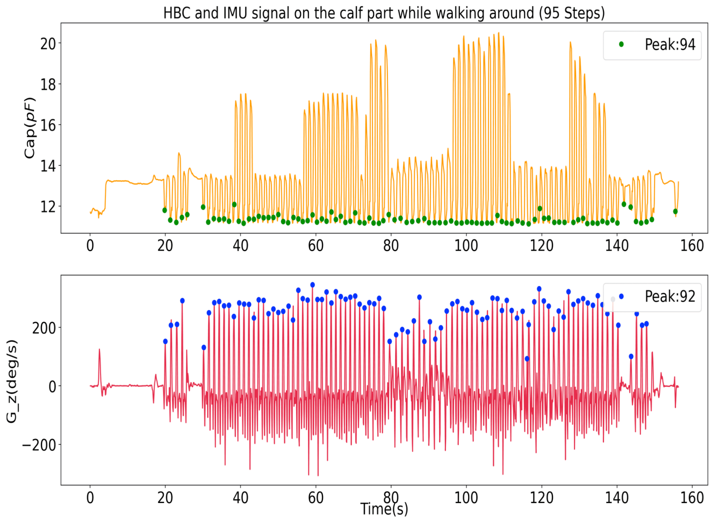

Fig. 15. Peak detection for step counting

data is 1.0 pF smaller than the sampled data 1 s ago, and is 1 s away from the last peak. The detection method can be accomplished by only one or two instructions in code. For the gyroscope signal, we tried different peak detection methods, including the same method as the capacitance one, and the *find_peaks* function from SciPy library [36] shows the best accuracy, with which we defined the prominence of the function as 200 (the prominence of a peak measures how much a peak stands out from the surrounding baseline of the signal and is defined as the vertical distance between the peak and its lowest contour line). Table 8 gives the peak detection result from the ten sessions data sets, the capacitance signal supplies the highest step counting accuracy with 99.4%.

Table 8. Step counting with signal from gyroscope and body-capacitance

Sets	1	2	3	4	5	6	7	8	9	10	Over all (accuracy)
Practical step	95	101	125	98	89	85	96	121	105	83	998 (100%)
Gyroscope z-axis	92	100	120	90	85	80	91	110	98	75	941 (94.3%)
Capacitance	94	101	126	97	88	85	95	119	104	83	992 (99.4%)

Compared with the movement sensor supplied step signals, the capacitance sensing unit supplies a more clear signal of each step firstly. As a result, the step number can be algorithmically easily captured with high accuracy. Secondly, the capacitance sensing unit supplies also the ground information, which is beyond the capability of the motion sensors. In Fig. 14, four types of ground could be derived simply by reading the amplitude of the capacitance signal. The volunteer walked on the textile floor in three periods, from 19 s to 38 s, from 43 s to 56 s, from 138 s to 151 s, 29 steps all together. Also three periods during carpet floor: 38 s to 43 s, 56 s to 72 s, and 134 s to 138 s, 19 steps all together. And three periods during concrete floor: 74 s to 80 s, 96 s to 111 s, and 127 s to 132 s, 19 steps all together. Two periods during wood floor: 80 s to 96 s and 112 s to 127 s, 22 steps all together. The steps are read directly by counting the peaks. Besides those periods, there are also some time points locating at the transition state, for example, 72 s to 74 s, during which the tester was on the textile floor (located between a carpet and concrete floor). Benefitting from the body's electric property in capacitance, tasks of exact step counting and potentially ground classification can be implemented (as we described above). When combining this sensing modality with the motion sensor, more accurate gait analysis and indoor location work would also be interesting topics.

5.2 Gait Partitioning

Gait monitoring is used widely in clinical practice for the evaluation of abnormal gait caused by disease, like Parkinson's disease [37–39]; multiple sclerosis [40–42]; attention deficit hyperactivity disorder [43–45], etc. Among the gait-related parameters, the temporal parameters (stride duration, stance duration, and swing duration) are the mostly evaluated ones because of their intensive connection to the gait abnormalities [46,47]. Whereas the stride length, gait speed is more related to estimate the walk trajectory [48–50]. The exact partitioning of the gait event is always the first step in gait analysis.

A variety of sensors can be used for gait phase partitioning, as summarized by Taborri et al. [51]. The most widely used sensor is the inertial sensor, like accelerometer [52,53], gyroscope [54,55], or IMU [56,57]. The inertial sensor wins quantitatively in the number of works because of its competitive advantages in size, cost, power consumption, and wearable capability. According to Taborri's survey, around two-thirds of gait analysis studies (among the 72 studies) relied on the inertial sensors. Anyway, to discriminate the gait event, the inertial sensor-based approach suffers from its computational load, accumulated drift over time, and also the necessary calibration procedure. Another popular gait partitioning approach is to use the footswitches [58] or foot pressure insole [59,60]. Both are based on force-sensitive sensors and require simple signal conditioning as well as post-processing. They could provide high accuracy in gait phase detection, which is reasonable since the gold standard in gait discrimination is represented by the foot's direct contact with the ground during a gait cycle. Besides those two approaches, some other sensing modalities were explored, like electromyography [61,62], ultrasound sensors [63], optoelectronic sensors [64]. Those marginally proposed approaches could give accurate partitioning results, but they are not feasible approaches for out-of-lab and long-term gait monitoring.

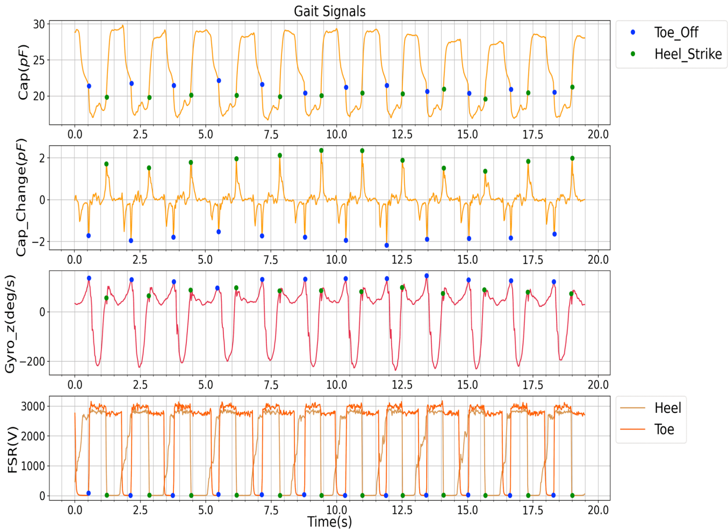

Fig. 16. Gait events detection with sensors of FSR, capacitance and gyroscope

As we described above, body capacitance variation during a walk can supply the gait event information directly and explicitly. This subsection presents a novel approach for gait partitioning (stance phase and swing phase) by utilizing the variation of human body capacitance during the walk. We firstly deployed the prototype (as depicted in Fig. 13) at the lower calf, with the sensing electrode attached to the skin and the locally grounded conductive tap beneath the shoe sole. Meanwhile, we added two FSR (Force Sensitive Sensor [65]) to the underside of the shoe sole (at the front and end position of the shoe sole), aiming to sense the contact of heel and toe to the ground and to supply the ground truth of the gait partitioning test. As described in [51], the direct measurements of the contact between foot and ground by force-sensitive sensors are often used as a gold standard for the validation of other methodologies. In this study, five volunteers walked around our office place with a regular speed for around one and a half minutes by wearing the prototype on the right calf. The sample rate of all the signals in this study is 50 Hz. Figure 16 depicts the sensed signals from FSR, z-axis of gyroscope, and the capacitance prototype. Among the six signals supplied by the IMU (three axes of the accelerometer, three axes of the gyroscope), z-axis of the gyroscope gives the most reliable source, which is also demonstrated by other works [32,51,66]. The algorithm we used to detect the heel-strike and toe-off from the gyroscope signal is a rule-based algorithm, which was described by Catalfamo et al. in [67] (with some calibration of the corresponding parameters), where the success rate for heel-strike and toe-off was over 98%. The ground truth was supplied by the two FSR, where the contact of the FSR to the ground could be easily detected by simply observing the voltage on the FSR. Once the voltage drops to zero (resistance of the FSR drops to zero), the contact happened. The gait event detection from the capacitance signal was attained by observing the change (the second subplot of Fig. 16) of the observed capacitance value (the first subplot of Fig. 16), utilizing the same algorithm described in [67]. To be noticed, the signal of z-axis of the gyroscope from Fig. 15 and Fig. 16 is not in the same pattern simply because of the prototype's orientation difference during the experiments. Overall, we recognized 523 steps from the FSR, 521 steps from the capacitance prototype, and 501 steps from the z-axis of the gyroscope with the above-described methods. To compare the performance of the gait event detection and gait phase partitioning from different signal sources, we synchronized all the detected steps from the three signal sources, meaning that the steps without the successful detection of all the three sensing approaches are discarded.

Table 9. Gait event sensing time error with signals of Cap and Gyro (FSR source as ground-truth)

Gait event and signal source	Heel strike, cap	Heel strike, gyro	Toe off, cap	Toe off, gyro
Mean(s)	−0.002	−0.022	0.043	0.040
Standard deviation(s)	0.010	0.014	0.009	0.019

Figure 17 depicted the gait event detection's time error distribution from the capacitance sensing and gyroscope sensing with a Boxplot [68]. The FSR approach supplies the ground truth. The heel-strike detection by the capacitance signal is significantly more accurate than the detection by the gyroscope z-axis signal since the majority of the time error from the capacitance signal locates in

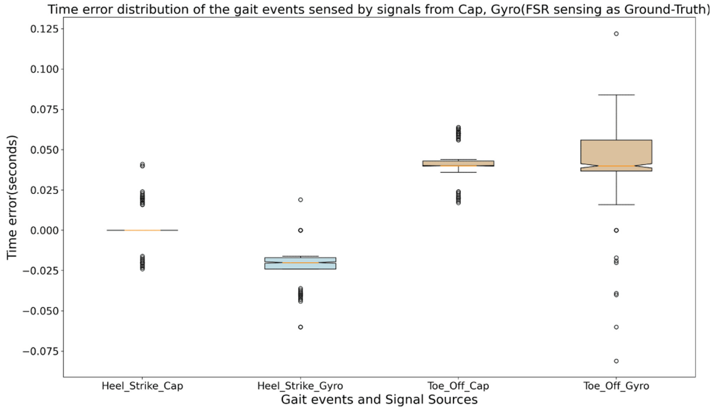

Fig. 17. Time error of Heel_Strike and Toe_Off with sensing source of capacitance and gyroscope

the field of the ground truth. For the event of toe-off, although most time errors from both capacitance and gyroscope sensors have an error of around 40 ms, the capacitance approach shows a much stable result. The same result could also be viewed by the mean and standard deviation of the errors from Table 9, where the mean error of the capacitance-based heel-strike detection is only two milliseconds. The gait event detection shows that the human body capacitance could be a reliable signal source for gait partitioning.

Based on the above analysis, we calculated the stance phase and swing phase's duration in each step after the gait partitioning by each signal source. The Box-plot in Fig. 18 shows the distribution of sensed stance and swing duration in seconds. The duration of both stance and swing phases detected by the capacitance prototype is closer to the ground truth (supplied by FSR) than the duration sensed by the gyroscope. As Table 10 lists, the mean duration of stance and swing phase from the FSR is 0.903 s and 0.674 s, respectively, the capacitance sensing gives 0.945 s and 0.632 s for each phase, with a mean accuracy of 95.3% and 93.7%, which is higher than the mean accuracy of the gyroscope-based stance and swing duration detection (93.1% and 90.8%).

Table 10. Gait phase duration with signals of FSR, Cap and Gyro

Gait phase and signal source	Stance, FSR	Stance, cap	Stance, gyro	Swing, FSR	Swing, cap	Swing, gyro
Mean(s)	0.903	0.945	0.965	0.674	0.632	0.612
Standard deviation(s)	0.041	0.040	0.045	0.035	0.036	0.038

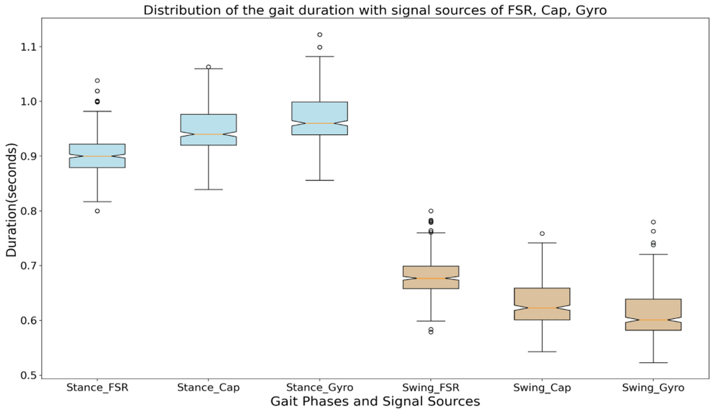

Fig. 18. Duration of stance and swing

The gait partitioning evaluation with our prototype demonstrated that the human body capacitance is a reliable signal source for gait partitioning. Our new approach is more simple (vs. force-based approach, only one small grounded electrode is needed), lower-cost (vs. force-based approach), and more accurate (vs. initial measurement unit).

5.3 Touch Sensing

Current *HBC* related capacitive sensing applications mostly focused on proximity sensing [3,69,70], activity recognition [24,71–73]. Another body-utilized capacitance application, probably one of the oldest, easiest, and most useful applications is touch sensing [74,75]. The most widely used capacitive touch sensing application is the capacitive touch button [76] and touch screen [77] for decades. Those applications are mostly based on the induced current on the sensing unit mounted on the touched object, caused by finger-touch. Different electrode layouts enlarged its touching scenarios [78]. With our prototype deployed at the lower calf (as Fig. 13 depicts), we utilized the body capacitance for touch sensing with the sensing unit on the body, approached the awareness of touch sensing at the executor side, instead of the receptor side as the previous work described.

Figure 19 shows the capacitance signal when touching the different objects within the working office. Three times handshakes caused the first three peaks (1 s to 8 s). From 9 s to 20 s, the executor touched a ground-standing metal frame, and a second volunteer touched the frame at a different position three times. The executor could sense the touch-action from the second volunteer. This sensing ability could be used for cooperation activity detection in an industrial manufactory, where the presence of the hand from a second colleague needs to be detected while processing the same objects. From 22 s to 31 s, 38 s to 44 s, 55 s to 62 s, and 69 s to 76 s, the executor touched the earthed computer, the whiteboard, the wall and the glass window for three times separately. While touching the earthed or good earth-coupled object, the prototype could perceive a visible touch signal. The wall and the window could be sensed by touching since they both are good earth-coupled through the concrete reinforcing bars and metal window frames. The deep peaks in the figure are signals of foot movement. The described touch sensing is a passive, intrusive one, and without the need of deploying the sensing unit near the touch point. Here we only present a primary observation aiming to present the potential ability of the researched object, a quantitative analysis will be presented in the future.

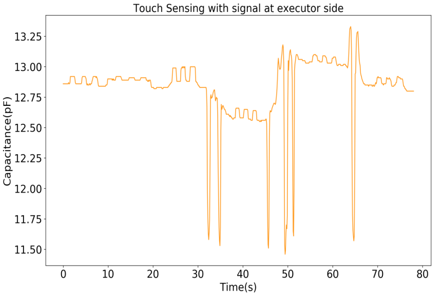

Fig. 19. Touch signal at the executor side

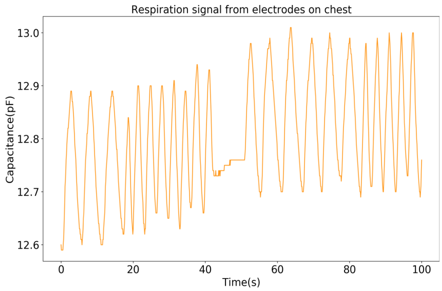

Fig. 20. Respiration signal

5.4 Respiration Monitoring

Respiration detection can be addressed by multiple ways [79], for example, by microphones, monitoring the loudness of the breath sound, or sensors that can analyze the air breathed out. Recently some novel methods were provided, like WIFI signal [80], ultra-wideband radar [81]. In our work, we use body capacitance to detect respiration, a wearable, and low-cost way. We attached the sensing electrode on the chest, and the local-ground of the prototype as a second electrode on another spot of the chest. The distance of the two electrodes was kept around 15 cm. In essence, this kind of deployment measures the local capacitance of part of the body, which was explained by Cheng [24] in detail, namely the local capacitance variation caused by the structure change inside the body.

Figure 20 recorded the capacitance signal in the level of sub-pF between the two on the chest attached electrodes. In the beginning, the volunteer breathed slowly and evenly three times, and then the respiration rate became faster. After eight times of breath, the volunteer held the breath for a while. The latter breath signal represents a repeat of the respiration in two rates. The scale of the signal variation represents the breath depth of the volunteer.

Similar applications can be explored by the same deployment but at other body parts. For example, when wearing the prototype on the wrist, with the sensing electrode attached to the finger, the local-ground electrode is also on the wrist, then the finger's movement can be observed. So as the head actions and other joint-related movements.

6 Conclusion

As one of the body's physiological variables, HBC is a pervasive signal worth further research. In this work, we first used a wearable prototype to measure the value of HBC in static and dynamic body states and got a reliable result. We also validated that the factors like postures, wearings, and environment can affect the value of HBC. Secondly, we briefly presented several body capacitance-based use cases with the wearable prototype, including ground type recognition (F-score of 0.63), exact step counting (with 99.4% accuracy), gait partitioning (with the duration accuracy of 95.3% and 93.7% for stance and swing phases, respectively), touch sensing, and respiration monitoring. Compared with traditional motion sensors, the HBC based sensing approach supplies body-related motion detection with competitive performance and the sensing ability for environmental and other physiological information. Future work will be focused on the HBC-based use cases exploration with a quantitative way, aiming to present a solid contribution of this signal.

References

1. Skeldon, K.D., Reid, L.M., McInally, V., Dougan, B., Fulton, C.: Physics of the Theremin. Am. J. Phys. **66**(11), 945–955 (1998)
2. Fritz, T.: ThereminVision-II instruction manual (2004)
3. Arshad, A., Khan, S., Alam, A.H.M.Z., Kadir, K.A., Tasnim, R., Ismail, A.F.: A capacitive proximity sensing scheme for human motion detection. In: 2017 IEEE International Instrumentation and Measurement Technology Conference (I2MTC), pp. 1–5. IEEE (2017)
4. Hirsch, M., Cheng, J., Reiss, A., Sundholm, M., Lukowicz, P., Amft, O.: Hands-free gesture control with a capacitive textile neckband. In: Proceedings of the 2014 ACM International Symposium on Wearable Computers, pp. 55–58 (2014)
5. Bian, S., Lukowicz, P.: Capacitive sensing based on-board hand gesture recognition with TinyML. In: UbiComp-ISWC 2021 Adjunct: Adjunct Proceedings of the 2021 ACM International Joint Conference on Pervasive and Ubiquitous Computing and Proceedings of the 2021 ACM International Symposium on Wearable Computers, Virtual, USA. ACM, September 2021
6. Cohn, G., Morris, D., Patel, S., Tan, D.: Humantenna: using the body as an antenna for real-time whole-body interaction. In: Proceedings of the SIGCHI Conference on Human Factors in Computing Systems, pp. 1901–1910 (2012)
7. Aliau Bonet, C., Pallàs Areny, R.: A fast method to estimate body capacitance to ground. In: Proceedings of XX IMEKO World Congress 2012, Busan, South Korea, 9–14 September 2019, pp. 1–4 (2012)
8. Aliau-Bonet, C., Pallas-Areny, R.: A novel method to estimate body capacitance to ground at mid frequencies. IEEE Trans. Instrum. Meas. **62**(9), 2519–2525 (2013)

9. Buller, W., Wilson, B.: Measurement and modeling mutual capacitance of electrical wiring and humans. IEEE Trans. Instrum. Meas. **55**(5), 1519–1522 (2006)
10. Forster, I.C.: Measurement of patient body capacitance and a method of patient isolation in mains environments. Med. Biol. Eng. **12**(5), 730–732 (1974). https://doi.org/10.1007/BF02477239
11. Greason, W.D.: Quasi-static analysis of electrostatic discharge (ESD) and the human body using a capacitance model. J. Electrostat. **35**(4), 349–371 (1995)
12. Huang, J., Wu, Z., Liu, S.: Why the human body capacitance is so large. In: Proceedings Electrical Overstress/Electrostatic Discharge Symposium, pp. 135–138. IEEE (1997)
13. Pallas-Areny, R., Colominas, J.: Simple, fast method for patient body capacitance and power-line electric interference measurement. Med. Biol. Eng. Comput. **29**(5), 561–563 (1991). https://doi.org/10.1007/BF02442332
14. Sălceanu, A., Neacşu, O., David, V., Luncă, E.: Measurements upon human body capacitance: theory and experimental setup (2004)
15. Jonassen, N.: Human body capacitance: static or dynamic concept? [ESD]. In: Electrical Overstress/Electrostatic Discharge Symposium Proceedings 1998 (Cat. No. 98TH8347), pp. 111–117. IEEE (1998)
16. Fujiwara, O., Ikawa, T.: Numerical calculation of human-body capacitance by surface charge method. Electron. Commun. Jpn (Part I: Commun.) **85**(12), 38–44 (2002)
17. Serrano, R.E., Gasulla, M., Casas, O., Pallàs-Areny, R.: Power line interference in ambulatory biopotential measurements. In: Proceedings of the 25th Annual International Conference of the IEEE Engineering in Medicine and Biology Society (IEEE Cat. No. 03CH37439), vol. 4, pp. 3024–3027. IEEE (2003)
18. Haberman, M., Cassino, A., Spinelli, E.: Estimation of stray coupling capacitances in biopotential measurements. Med. Biol. Eng. Comput. **49**(9) (2011). Article number: 1067. https://doi.org/10.1007/s11517-011-0811-6
19. Fish, R.M., Geddes, L.A.: Conduction of electrical current to and through the human body: a review. Eplasty **9**, e44 (2009)
20. TI: Texas Instrument LMC555, June 2016. http://www.ti.com/lit/ds/symlink/lmc555.pdf
21. TI: How do i design a-stable timer, oscillator, circuits using LMC555, TLC555, LM555, NA555, NE555, SA555, or SE555. https://e2e.ti.com/support/clock-andtiming/f/48/t/879112?tisearch=e2e-sitesearchamp;keymatch=lmc555
22. PJRC: Teensy 3.6. https://www.pjrc.com/store/teensy36.html
23. Grosse-Puppendahl, T.: Capacitive sensing and communication for ubiquitous interaction and environmental perception. Ph.D. thesis, Technische Universität (2015)
24. Cheng, J., Amft, O., Bahle, G., Lukowicz, P.: Designing sensitive wearable capacitive sensors for activity recognition. IEEE Sens. J. **13**(10), 3935–3947 (2013)
25. Castle, G.S.P.: Contact charging between insulators. J. Electrostat. **40**, 13–20 (1997)
26. Electrostatic-Discharge-Association: Handbook for the Development of an Electrostatic Discharge Control Program for the Protection of Electronic Parts, Assemblies, and Equipment. TR20.20-2016
27. Pedregosa, F., et al.: Scikit-learn: machine learning in Python. J. Mach. Learn. Res. **12**, 2825–2830 (2011)
28. Chawla, N.V., Bowyer, K.W., Hall, L.O., Kegelmeyer, W.P.: SMOTE: synthetic minority over-sampling technique. J. Artif. Intell. Res. **16**, 321–357 (2002)

29. Kuhn, M., Johnson, K.: Feature Engineering and Selection: A Practical Approach for Predictive Models. CRC Press, Boca Raton (2019)
30. Foster, R.C., et al.: Precision and accuracy of an ankle-worn accelerometer-based pedometer in step counting and energy expenditure. Prev. Med. **41**(3–4), 778–783 (2005)
31. Pan, M.-S., Lin, H.-W.: A step counting algorithm for smartphone users: design and implementation. IEEE Sens. J. **15**(4), 2296–2305 (2014)
32. Rhudy, M.B., Mahoney, J.M.: A comprehensive comparison of simple step counting techniques using wrist-and ankle-mounted accelerometer and gyroscope signals. J. Med. Eng. Technol. **42**(3), 236–243 (2018)
33. Do, T.-N., Liu, R., Yuen, C., Tan, U.-X.: Design of an infrastructureless in-door localization device using an IMU sensor. In: 2015 IEEE International Conference on Robotics and Biomimetics (ROBIO), pp. 2115–2120. IEEE (2015)
34. Ashkar, R., Romanovas, M., Goridko, V., Schwaab, M., Traechtler, M., Manoli, Y.: A low-cost shoe-mounted inertial navigation system with magnetic disturbance compensation. In: International Conference on Indoor Positioning and Indoor Navigation, pp. 1–10. IEEE (2013)
35. Mariani, B., Hoskovec, C., Rochat, S., Büla, C., Penders, J., Aminian, K.: 3D gait assessment in young and elderly subjects using foot-worn inertial sensors. J. Biomech. **43**(15), 2999–3006 (2010)
36. Virtanen, P., et al.: SciPy 1.0: fundamental algorithms for scientific computing in Python. Nat. Methods **17**, 261–272 (2020)
37. Sofuwa, O., Nieuwboer, A., Desloovere, K., Willems, A.-M., Chavret, F., Jonkers, I.: Quantitative gait analysis in Parkinson's disease: comparison with a healthy control group. Arch. Phys. Med. Rehabil. **86**(5), 1007–1013 (2005)
38. Salarian, A., et al.: Gait assessment in Parkinson's disease: toward an ambulatory system for long-term monitoring. IEEE Trans. Biomed. Eng. **51**(8), 1434–1443 (2004)
39. Pedersen, S.W., Oberg, B., Larsson, L.E., Lindval, B.: Gait analysis, isokinetic muscle strength measurement in patients with Parkinson's disease. Scand. J. Rehabil. Med. **29**(2), 67–74 (1997)
40. Givon, U., Zeilig, G., Achiron, A.: Gait analysis in multiple sclerosis: characterization of temporal-spatial parameters using GAITRite functional ambulation system. Gait Posture **29**(1), 138–142 (2009)
41. Benedetti, M.G., Piperno, R., Simoncini, L., Bonato, P., Tonini, A., Giannini, S.: Gait abnormalities in minimally impaired multiple sclerosis patients. Multiple Sclerosis J. **5**(5), 363–368 (1999)
42. Guner, S., Inanici, F.: Yoga therapy and ambulatory multiple sclerosis assessment of gait analysis parameters, fatigue and balance. J. Bodyw. Mov. Ther. **19**(1), 72–81 (2015)
43. Buderath, P., et al.: Postural and gait performance in children with attention deficit/hyperactivity disorder. Gait Posture **29**(2), 249–254 (2009)
44. Papadopoulos, N., McGinley, J.L., Bradshaw, J.L., Rinehart, N.J.: An investigation of gait in children with attention deficit hyperactivity disorder: a case controlled study. Psychiatry Res. **218**(3), 319–323 (2014)
45. Leitner, Y., et al.: Gait in attention deficit hyperactivity disorder. J. Neurol. **254**(10), 1330–1338 (2007). https://doi.org/10.1007/s00415-006-0522-3
46. Morris, M.E., Matyas, T.A., Iansek, R., Summers, J.J.: Temporal stability of gait in Parkinson's disease. Phys. Ther. **76**(7), 763–777 (1996)

47. Trojaniello, D., Ravaschio, A., Hausdorff, J.M., Cereatti, A.: Comparative assessment of different methods for the estimation of gait temporal parameters using a single inertial sensor: application to elderly, post-stroke, Parkinson's disease and Huntington's disease subjects. Gait Posture **42**(3), 310–316 (2015)
48. Hori, K., et al.: Inertial measurement unit-based estimation of foot trajectory for clinical gait analysis. Front. Physiol. **10**, 1530 (2019)
49. Hu, X., Huang, Z., Jiang, J., Qu, X.: An inertial sensor based system for real-time biomechanical analysis during running. J. Med. Bioeng. **6**(1), 1–5 (2017)
50. Woyano, F., Lee, S., Park, S.: Evaluation and comparison of performance analysis of indoor inertial navigation system based on foot mounted IMU. In: 2016 18th International Conference on Advanced Communication Technology (ICACT), pp. 792–798. IEEE (2016)
51. Taborri, J., Palermo, E., Rossi, S., Cappa, P.: Gait partitioning methods: a systematic review. Sensors **16**(1), 66 (2016)
52. Selles, R.W., Formanoy, M.A.G., Bussmann, J.B.J., Janssens, P.J., Stam, H.J.: Automated estimation of initial and terminal contact timing using accelerometers; development and validation in transtibial amputees and controls. IEEE Trans. Neural Syst. Rehabil. Eng. **13**(1), 81–88 (2005)
53. Han, J., Jeon, H.S., Jeon, B.S., Park, K.S.: Gait detection from three dimensional acceleration signals of ankles for the patients with Parkinson's disease. In: Proceedings of the IEEE The International Special Topic Conference on Information Technology in Biomedicine, Ioannina, Epirus, Greece, vol. 2628 (2006)
54. Formento, P.C., Acevedo, R., Ghoussayni, S., Ewins, D.: Gait event detection during stair walking using a rate gyroscope. Sensors **14**(3), 5470–5485 (2014)
55. Darwin Gouwanda and Alpha Agape Gopalai: A robust real-time gait event detection using wireless gyroscope and its application on normal and altered gaits. Med. Eng. Phys. **37**(2), 219–225 (2015)
56. Lau, H., Tong, K.: The reliability of using accelerometer and gyroscope for gait event identification on persons with dropped foot. Gait Posture **27**(2), 248–257 (2008)
57. Kotiadis, D., Hermens, H.J., Veltink, P.H.: Inertial gait phase detection for control of a drop foot stimulator: inertial sensing for gait phase detection. Med. Eng. Phys. **32**(4), 287–297 (2010)
58. Agostini, V., Balestra, G., Knaflitz, M.: Segmentation and classification of gait cycles. IEEE Trans. Neural Syst. Rehabil. Eng. **22**(5), 946–952 (2013)
59. Lie, Yu., Zheng, J., Wang, Y., Song, Z., Zhan, E.: Adaptive method for real-time gait phase detection based on ground contact forces. Gait Posture **41**(1), 269–275 (2015)
60. Kim, H., Kang, Y., Valencia, D.R., Kim, D.: An integrated system for gait analysis using FSRs and an IMU. In: 2018 Second IEEE International Conference on Robotic Computing (IRC), pp. 347–351. IEEE (2018)
61. Lauer, R.T., Smith, B.T., Coiro, D., Betz, R.R., McCarthy, J.: Feasibility of gait event detection using intramuscular electromyography in the child with cerebral palsy. Neuromodulation Technol. Neural Interface **7**(3), 205–213 (2004)
62. Joshi, C.D., Lahiri, U., Thakor, N.V.: Classification of gait phases from lower limb EMG: application to exoskeleton orthosis. In: 2013 IEEE Point-of-Care Healthcare Technologies (PHT), pp. 228–231. IEEE (2013)
63. Qi, Y., Soh, C.B., Gunawan, E., Low, K.-S., Thomas, R.: Assessment of foot trajectory for human gait phase detection using wireless ultrasonic sensor network. IEEE Trans. Neural Syst. Rehabil. Eng. **24**(1), 88–97 (2015)

64. Galois, L., Girard, D., Martinet, N., Delagoutte, J.P., Mainard, D.: Optoelectronic gait analysis after metatarsophalangeal arthrodesis of the hallux: fifteen cases. Rev. Chir. Orthop. Reparatrice Appar. Mot. **92**(1), 52–59 (2006)
65. OHMITE: FSR series force sensing resistor (2020)
66. Panebianco, G.P., Bisi, M.C., Stagni, R., Fantozzi, S.: Analysis of the performance of 17 algorithms from a systematic review: influence of sensor position, analysed variable and computational approach in gait timing estimation from IMU measurements. Gait Posture **66**, 76–82 (2018)
67. Catalfamo, P., Ghoussayni, S., Ewins, D.: Gait event detection on level ground and incline walking using a rate gyroscope. Sensors **10**(6), 5683–5702 (2010)
68. McGill, R., Tukey, J.W., Larsen, W.A.: Variations of box plots. Am. Stat. **32**(1), 12–16 (1978)
69. Braun, A., Hamisu, P.: Using the human body field as a medium for natural interaction. In: Proceedings of the 2nd International Conference on PErvasive Technologies Related to Assistive Environments, pp. 1–7 (2009)
70. Braun, A., Hamisu, P.: Designing a multi-purpose capacitive proximity sensing input device. In: Proceedings of the 4th International Conference on PErvasive Technologies Related to Assistive Environments, pp. 1–8 (2011)
71. Bian, S., Rey, V.F., Younas, J., Lukowicz, P.: Wrist-worn capacitive sensor for activity and physical collaboration recognition. In: 2019 IEEE International Conference on Pervasive Computing and Communications Workshops (PerCom Workshops), pp. 261–266. IEEE (2019)
72. Bian, S., Rey, V.F., Hevesi, P., Lukowicz, P.: Passive capacitive based approach for full body gym workout recognition and counting. In: 2019 IEEE International Conference on Pervasive Computing and Communications (PerCom), pp. 1–10. IEEE (2019)
73. Bian, S., Yuan, S., Rey, V.F., Lukowicz, P.: Using human body capacitance sensing to monitor leg motion dominated activities with a wrist worn device. In: Activity and Behavior Computing. Springer (2022)
74. Du, L.: An overview of mobile capacitive touch technologies trends. arXiv preprint arXiv:1612.08227 (2016)
75. Savage, V., Zhang, X., Hartmann, B.: Midas: fabricating custom capacitive touch sensors to prototype interactive objects. In: Proceedings of the 25th Annual ACM Symposium on User Interface Software and Technology, pp. 579–588 (2012)
76. Curtis, K., Perme, T.: Capacitive multibutton configurations (2007)
77. Leeper, A.K.: 14.2: integration of a clear capacitive touch screen with a 1/8-VGA FSTN-LCD to form and LCD-based touchpad. In: SID Symposium Digest of Technical Papers, vol. 33, pp. 187–189. Wiley Online Library (2002)
78. Baxter, L.K.: Capacitive Sensors: Design and Applications (1997)
79. AL-Khalidi, F.Q., Saatchi, R., Burke, D., Elphick, H., Tan, S.: Respiration rate monitoring methods: a review. Pediatr. Pulmonol. **46**(6), 523–529 (2011)
80. Wang, H., et al.: Human respiration detection with commodity wifi devices: do user location and body orientation matter? In: Proceedings of the 2016 ACM International Joint Conference on Pervasive and Ubiquitous Computing, pp. 25–36 (2016)
81. Li, X., Qiao, D., Li, Y., Dai, H.: A novel through-wall respiration detection algorithm using UWB radar. In: 2013 35th Annual International Conference of the IEEE Engineering in Medicine and Biology Society (EMBC), pp. 1013–1016. IEEE (2013)